

CHIMIE

146

NOUVELLE

LA REVUE DE CONTACT DE LA SOCIÉTÉ ROYALE DE CHIMIE

42^{ème} année - novembre 2024

SRC
SOCIÉTÉ ROYALE DE CHIMIE

Quantum Computing

**UV-vis vibronic absorption spectra simulation
by Doktorov Quantum Circuit**
R. OLARTE HERNANDEZ

1

Single Molecule Spectroscopy

**Investigating the mechanical stability of Diels-Alder
mechanophores by AFM-based single-molecule
force spectroscopy**
T. CARABIN - A.-S. DUWEZ

12

Directeurs de rédaction

Bernard Mahieu
UCLouvain, Ecole de Chimie
Place Pasteur, 1
Boîte L4.01.07
1348 Louvain-la-Neuve
bernard.mahieu@uclouvain.be

Benoît Champagne
UNamur,
Département de Chimie
Rue de Bruxelles, 61
5000 Namur
benoit.champagne@unamur.be

Cédric Malherbe
ULiège,
Département de Chimie
Quartier Agora,
Allée du Six Août, 11
4000 Liège 1
c.malherbe@uliege.be

Infographisme

emmanuel@norproduction.eu

Comité de rédaction

Kristin Bartik, ULB
Nicolas Blanchard, Université de Haute-Alsace-Université
de Strasbourg
Sophie Carencu, Sorbonne Université, Paris
Frédéric Castet, Université de Bordeaux
André Colas, Dow Corning
Damien Debecker, UCLouvain
Karolien De Wael, UAntwerpen
Philippe Dubois, U Mons
Anne-Sophie Duwez, ULiège
Gwilherm Evano, ULB
Danielle Fauque, Université de Paris Sud
Stéphane Gérard, Faculté de Pharmacie, Reims
Bernard Joris, ULiège
Sophie Laurent, U Mons
Tatjana Parac-Vogt, KU Leuven
Raphaël Robiette, UCLouvain
Cédric Samuel, École des Mines de Douai
Armand Soldera, Université de Sherbrooke
Johan Wouters, UNamur

Secrétariat

Violaine Sizaire
ULB
Avenue Franklin Roosevelt 50, CP 160/07 1050 Bruxelles
Tel : +32 2 650 52 08 Fax : +32 2 650 51 84 - email : src@ulb.be
Fortis : BE60 2100 4208 0470

Comité directeur

Conseil de gestion

Présidente	A.-S. Duwez, ULiège	asduwez@uliege.be
Vice-président	J.-P. Lecomte, DOW	j.lecomte@dow.com
Président sortant	L. Provins, UCB	laurent.provins@ucb.com
Secrétaire générale	C. Buess-Herman, ULB	Claudine.Buess-Herman@ulb.be
Trésorier	T. Randoux, Certech	thierry.randoux@certech.be
Délégué relations extérieures	P. Baekelmans, Solvay L. Provins, UCB	paul.baekelmans@solvay.com laurent.provins@ucb.be

Divisions

Chimie Médicinale	P. Francotte, ULiège	Pierre.Francotte@uliege.be
Chimie organique et bio-organique	G. Evano, ULB	gwilherm.evano@ulb.be
Jeunes Chimistes	Martin Blavier	martin.blavier@uliege.be
	Dorothee Brandt	dorothee.brandt@unamur.be
Histoire et Enseignement de la Chimie	B. Van Tiggelen	vantiggelen@memosciences.be
Délégué Essenscia Wallonie	C. Moucheron, ULB T. Randoux, Certech	Cecile.Moucheron@ulb.be Thierry.Randoux@certech.be

Sections locales

Bruxelles	G. Evano, ULB	Gwilherm.Evano@ulb.be
Louvain-la-Neuve	B. Elias, UCLouvain	benjamin.elias@uclouvain.be
Mons	P. Gerboux, U Mons	pascal.gerboux@umons.ac.be
Liège	A. S. Duwez, ULiège	asduwez@ulg.ac.be
Namur	J. Wouters, UNamur	johan.wouters@unamur.be

Membres protecteurs de la SRC

ALLNEX
CERTECH
EXXONMOBIL CHEMICAL
LHOIST
NovAliX
SOLVAY
TOTALENERGIES
UCB

Parution : trimestrielle

Avec le soutien du Fonds National de la Recherche Scientifique.
Les articles paraissant dans Chimie nouvelle sont repris
dans CHEMICAL ABSTRACTS

Editeur responsable : Claudine Buess-Herman,
ULB, CP 160/07,
avenue Roosevelt 50, 1050 Bruxelles

Les articles sont soumis à un processus de reviewing.
Les annonces publicitaires sont établies sous la responsabilité des firmes.

« CHIMIE NOUVELLE » est un titre déposé

ISSN 0771-730X

Renato OLARTE HERNANDEZ

PhD student under the supervision of Prof. A. Soldera
and Prof. B. Champagne

Laboratoire de Chimie Théorique, University of Namur,
Rue de Bruxelles, 61, B-5000 Namur, Belgium

Laboratory of Physical Chemistry of Matter Université de Sherbrooke,
Sherbrooke, QC J1K 2R1, Canada
renato.olartehernandez@unamur.be

UV-vis vibronic absorption spectra simulation by Doktorov Quantum Circuit

1. Introduction

When Feynman considered a computer capable of using quantum principles to perform quantum calculations effectively, he was paving the way for modern quantum computers. Despite being in their early stages, these machines are already operational for small tasks and offer advantages over their classical counterparts [1]. The use of quantum computers promises significant speed-ups for large systems and quantum calculations that quickly

become unscalable. For instance, calculating molecular properties becomes computationally challenging as the number of atoms or electrons increases. The Hilbert space grows exponentially, making memory storage impractical. To overcome this technological challenge, new quantum algorithms have been proposed, taking advantage of their quantum nature.

To cite some works, quantum algorithms for calculating electronic energies [2], excited state

Box 1. Qubit and Quantum Gates [15]

Contrary to the classical bit of information which only has two discrete values, the quantum bit (qubit) can be in a continuous complex superposition of the $|0\rangle$ state and the $|1\rangle$ state. Further advantages when using several qubits such as entanglement allow to better express and effectively exploit the searched Hilbert space. To modify the circuit quantum state, logical quantum gates are used. Reminiscent of a logical or electrical circuit, the quantum gates are unitary operations that modify the state of the qubit(s). Among the most popular ones, there is the Hadamard gate, the CNOT gate, and the usual Pauli tensors X, Y, and Z. For instance, the Pauli X gate acts as a Not logical gate:

$$X|0\rangle = \begin{pmatrix} 0 & 1 \\ 1 & 0 \end{pmatrix} \begin{pmatrix} 1 \\ 0 \end{pmatrix} = \begin{pmatrix} 0 \\ 1 \end{pmatrix} = |1\rangle$$

And the Hadamard gate creates a uniform superposition:

$$H|0\rangle = \frac{1}{\sqrt{2}} \begin{pmatrix} 1 & 1 \\ 1 & -1 \end{pmatrix} \begin{pmatrix} 1 \\ 0 \end{pmatrix} = \frac{1}{\sqrt{2}} \begin{pmatrix} 1 \\ 1 \end{pmatrix} = \frac{|0\rangle + |1\rangle}{\sqrt{2}}$$

Applying gates one after another, can be visually represented by a quantum circuit.

energies [3], nonlinear molecular properties [4], and vibronic absorption signatures [5, 6] have been proposed. In this article, the aim is to simulate vibronic (electronic and vibrational) absorption spectra resulting from ionizations. The idea is to use Doktorov's second quantization operator \hat{U}_{Dok} , which encodes all the necessary information to calculate the vibronic signature. The operator is then translated into a series of quantum gates, yielding the final quantum circuit, also known as the *ansatz*. For illustrative purposes, the method is applied to the SO_2 and ZnOH molecules. Nevertheless, this method has the novelty and advantage of being general, and in principle, it could be applied to any size molecule and any symmetry point group.

This article starts with a theoretical review of the concepts behind vibronic spectroscopy and the methods used for the quantum algorithm setup, followed by a brief description of the simulated results and their comparison to other classical algorithms. Nevertheless, the Theory and Results sections can be read together and considered a milestone in quantum computation applications.

2. Theory

Calculating the intensity of vibronic transitions is computationally expensive because it requires estimating the Franck-Condon (FC) factors. These factors arise from Fermi's Golden Rule under the Born-Oppenheimer approximation, where the total wave function can be separated into its electronic and vibrational components $|\psi\rangle = |\psi^e\rangle \otimes |\psi^{\text{vib}}\rangle$ and the Condon approximation allows to rewrite the dipole moment operator as $\hat{\mu} = \hat{\mu}_e + \hat{\mu}_N$. After some transformations, the probability I of a photon-induced transition from the ground state 1 to a certain state 2 is:

$$I \propto \text{FC}_{1 \rightarrow 2} |\langle \psi_2^e | \hat{\mu}_e | \psi_1^e \rangle|^2$$

where the $\text{FC}_{1 \rightarrow 2} = |\langle \psi_2^{\text{vib}} | \psi_1^{\text{vib}} \rangle|^2$ is the FC factor. It corresponds to the overlap of the nuclear wavefunctions modulus squared. A visual representation of these factors is shown in Fig. 1.

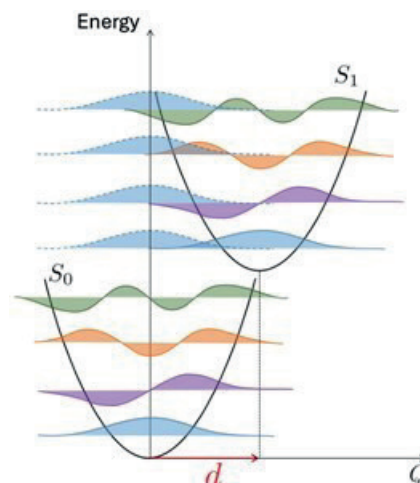


Figure 1. Graphical representation of the Franck-Condon factors for one normal mode. The ground state nuclear wavefunction is projected to the different vibronic states.

Where Q is the normal mode coordinate and d the translational shift between the ground and excited potential energy surfaces (PES) for that normal mode. These FC integrals fulfill the very useful property:

$$\sum_{\nu} \text{FC}_{1 \rightarrow 2}(\nu) = 1$$

where the sum is over all the possible vibronic transitions ν . It allows monitoring how much the vibrational contributions are considered. Calculating the overlap of the (bosonic) nuclear wavefunctions is not straightforward because the initial ground state and the final state are not expressed in the same basis. Classically, the initial and final vibrational normal mode coordinate vectors, \vec{q}_i and \vec{q}_f respectively, are related by the Duschinsky transformation:

$$\vec{q}_f = U_D \vec{q}_i + \vec{d}$$

where U_D is the Duschinsky rotational matrix that mixes the L vibrational normal modes, and \vec{d} is the displacement vector. When considering an electronic transition, such as an ionization, the Duschinsky transformation relates the ground and excited PES of all the different normal modes.

Besides translation and rotation, another important aspect is accounting for frequency squeezing: under the harmonic approximation, the ground and excited state normal mode frequencies differ. These three major transformations can be applied via the Doktorov operator \hat{U}_{Dok} to transform the final state 2 into its equivalent but expressed in the ground state basis:

$$\text{FC}_{1 \rightarrow 2} = |\langle \psi_{2f}^{\text{vib}} | \psi_{1i}^{\text{vib}} \rangle|^2 = |\langle \psi_{2i}^{\text{vib}} | \hat{U}_{\text{Dok}} | \psi_{1i}^{\text{vib}} \rangle|^2$$

where for the sake of clarity, the subscript indicating the basis was added. After some algebraic manipulations, the Doktorov operator can be written as:

$$\hat{U}_{\text{Dok}} = \hat{U}_t \hat{U}_s \hat{U}_r = \prod_l^L \hat{U}_{t,l} \prod_l^L \hat{U}_{s,l} \hat{U}_r$$

where the translation and squeezing have been decoupled such that every normal mode l , among the $L=3N-6$, is affected by one translational and one squeezing operator:

$$\hat{U}_{t,l} = \exp\left(\frac{d_l \sqrt{\omega_{2,l}}}{\sqrt{2}\hbar} (\hat{b}_l^\dagger - \hat{b}_l)\right) = \exp(\alpha_l (\hat{b}_l^\dagger - \hat{b}_l))$$

$$\hat{U}_{s,l} = \exp\left(\frac{1}{4} \ln(\omega_{2,l}/\omega_{1,l}) (\hat{b}_l^\dagger \hat{b}_l^\dagger - \hat{b}_l \hat{b}_l)\right) = \exp(\beta_l (\hat{b}_l^\dagger \hat{b}_l^\dagger - \hat{b}_l \hat{b}_l))$$

where $\omega_{1,l}$ and $\omega_{2,l}$ are the normal mode frequencies of the ground and excited state respectively, and \hat{b}_l^\dagger and \hat{b}_l are (bosonic) harmonic nuclear creation and annihilation operators. Moreover, the dimensionless coefficients have been defined:

$$\alpha_l = \frac{d_l \sqrt{\omega_{2,l}}}{\sqrt{2}\hbar} \quad \text{and} \quad \beta_l = \frac{1}{4} \ln(\omega_{2,l}/\omega_{1,l}),$$

which will be pertinent for the ansatz parametrization *i.e.*, these constants will be calculated once and easily called for the trotterization code. The remaining rotational operator couples the normal modes among themselves. In the work presented here, involving three-atom molecules, the rotational operator is simplified to the case where only the first two normal modes are coupled. The mixing of the third normal mode is either excluded for symmetry reasons or neglected. The final expression for the rotational operator is:

$$\hat{U}_r = \exp[\theta(\hat{b}_2^\dagger \hat{b}_1 - \hat{b}_2 \hat{b}_1^\dagger)]$$

where θ is the angle of rotation of the two-dimensional Duschinsky matrix. These are the operators that need to be implemented on a quantum circuit to calculate the FC factors.

Box 2. Second Quantization

In the usual first quantization representation, quantum systems are described by continuous wavefunctions and operators such as the kinetic energy operator and potential energy operator. After a (rather tedious) change of basis, the wavefunction and operators can be expressed in their second quantization form: the wavefunction is now quantized, and ladder operators are used. For instance, when working with electrons within the harmonic approximation, the fermionic creation and annihilation operators, \hat{a}^\dagger and \hat{a} respectively, satisfy the commutation rules:

$$[\hat{a}, \hat{a}^\dagger] = \hat{1}$$

Such that

$$\hat{a}^\dagger|0\rangle = |1\rangle, \hat{a}^\dagger|1\rangle = 0 \text{ and} \\ \hat{a}|1\rangle = |0\rangle, \hat{a}|0\rangle = 0$$

The electronic wavefunction is represented by a chain of zeros and ones, indicating the presence or absence of an electron in each fermionic state, typically a spin-orbital. Exciting an electron from a state i to a state j , is easily comprehended as the simple excitation $\hat{a}_j^\dagger \hat{a}_i$.

3. Methods

The idea in this section is to translate the algebraic expression of the Doktorov operator into a quantum circuit. The two main steps are the bosonic mapping and the trotterization method. A final hybrid method is also described to retrieve the FC factors after statistical quantum measurement.

3.1. Bosonic encoding and mapping

The harmonic ladder bosonic operators are expressed in the usual Fock basis $\{|n\rangle\}_{n \in \mathbb{N}}$, meaning that every normal mode l can be represented by a n_l number representing the number of quanta on that specific mode. The total nuclear wavefunction for a three-atom molecule is written:

$$|\psi_i^{\text{vib}}\rangle = |n_3\rangle \otimes |n_2\rangle \otimes |n_1\rangle = |n_3, n_2, n_1\rangle$$

In practice, the quanta number n_l must be truncated. The choice of encoding and the number of allocated qubits determine how many vibrational quanta can be represented. There are two main encoding families: compact and noncompact [7]. For simplicity, the compact standard binary encoding is used. The quanta vibrational number is written as its binary representation. When choosing, for instance, to allocate $M=3$ qubits per normal mode,

it allows to represent $2^M=8$ vibrational quanta, one for the ground state and the remaining seven excitations for that normal mode. Representing a state with zero, one and seven excitations on the normal modes 1, 2 and 3 reads:

$$|7, 1, 0\rangle = |111, 001, 000\rangle = X_8 X_7 X_6 X_3 |0, 0, 0\rangle$$

To change a zero state to a one state it is enough to apply an X gate. This is how a vibrational wavefunction can be initialized.

The next step is to map the ladder operators into Pauli strings. The creation and annihilation operators can be represented in the Fock basis in their ket-bra decomposition. This means that they are linear combination of $|k\rangle\langle k'|$ matrices, where k and k' are truncated from 0 to 2^M-1 . It proceeds to do the same encoding as before: the k and k' numbers are converted into their binary representation, and after associating the corresponding *weight* qubits the following usual bosonic mapping is applied:

$$|0\rangle\langle 0| = \frac{1}{2}(I + Z), \quad |1\rangle\langle 1| = \frac{1}{2}(I - Z), \\ |1\rangle\langle 0| = \frac{1}{2}(X - iY), \quad |0\rangle\langle 1| = \frac{1}{2}(X + iY)$$

Box 3. Mapping [7]

When describing an equation or an operator in terms of unitary gates and qubits, it involves a mapping process. The translation to the language of quantum computers is not unique and depends on the specific system under study. When working with fermions, such as in electronic calculations, popular choices include the Jordan-Wigner mapping, the Bravyi-Kitaev transformation, the parity mapping, among others. For (quasi) bosons, the commutation rules differ, necessitating different mapping strategies. The choice of encoding system and mapping is crucial. The most common mapping is discussed here, but depending on factors such as locality, topology, or the Hamiltonian of the system, certain mappings may offer advantages over others.

For instance, when calculating the harmonic annihilation operator, which happens to be the same for all the vibrational normal modes:

$$\hat{b}_l = \begin{pmatrix} 0 & 1 & 0 & 0 & \dots \\ 0 & 0 & \sqrt{2} & 0 & \dots \\ 0 & 0 & 0 & \ddots & \dots \\ 0 & 0 & \dots & \ddots & \sqrt{7} \\ \dots & \dots & \dots & \dots & 0 \end{pmatrix}$$

One term appearing on the linear combination is:

$$\sqrt{2}|1\rangle\langle 2| = \sqrt{2}|001\rangle\langle 010| = \sqrt{2}|0\rangle\langle 0| \otimes |0\rangle\langle 1| \otimes |1\rangle\langle 0|$$

After mapping it becomes:

$$\begin{aligned} \sqrt{2}|0\rangle\langle 0| \otimes |0\rangle\langle 1| \otimes |1\rangle\langle 0| &= \sqrt{2} \frac{1}{2^3} (I_2 + Z_2)(X_1 + iY_1)(X_0 - iY_0) \\ &= \sqrt{2} \frac{1}{2^3} (X_1X_0 + Y_1Y_0 + Z_2X_1X_0 + Z_2Y_1Y_0 \\ &\quad + i(Y_1X_0 - X_1Y_0 + Z_2Y_1X_0 - Z_2X_1Y_0)) \end{aligned}$$

This term is composed of eight Pauli strings. Repeating this procedure for all the matrix terms gives the final expression of the annihilation operator with a three qubits truncation. The final expression is a combination of $\mathcal{O}(2^{2M})$ Pauli strings. Following this procedure, the translational, the squeezing and the rotational Doktorov operators can be expressed in a linear combination of Pauli terms.

3.2. Trotterization

Translating Doktorov operators into a quantum circuit is a non-trivial task. A closer examination of their expression reveals that these operators are complex exponentials of Pauli terms that do not commute with each other. However, due to their exponential form, the Trotterization method is appropriate [8]. In few words, the trotterization method allows the separation of two non-commuting operators, \hat{A} and \hat{B} , exponential, into two new exponentials of each operator:

$$e^{\hat{A}+\hat{B}} = \lim_{K \rightarrow \infty} (e^{\hat{A}/K} e^{\hat{B}/K})^K$$

The formula above is also known as the Lie product formula. The operators used here, are a linear combination of Pauli terms. With a qubit-wise approach, groups of commuting Pauli terms were determined. For instance, for the translational operator with three qubit truncation, three Pauli groups \hat{P}_i (each containing four commuting single Pauli strings $\hat{P}_{i,j}$) were determined, and the trotterization until a certain order K is:

$$\hat{U}_{t,l} \approx \left(e^{\frac{i\alpha_l \hat{p}_1}{K}} e^{\frac{i\alpha_l \hat{p}_2}{K}} e^{\frac{i\alpha_l \hat{p}_3}{K}} \right)^K$$

where α_l is the dimensionless constants defined previously. Taking into advantage of the inner commutation of the Pauli groups:

$$\hat{U}_{t,l} \approx \left(\prod_{j=1}^4 e^{\frac{i\alpha_l \hat{p}_{1,j}}{K}} \prod_{j=1}^4 e^{\frac{i\alpha_l \hat{p}_{2,j}}{K}} \prod_{j=1}^4 e^{\frac{i\alpha_l \hat{p}_{3,j}}{K}} \right)^K$$

This expression is exact with respect to the previous one. The key asset comes here, each of the single Pauli string exponentials $e^{\frac{i\alpha_l \hat{p}_{i,j}}{K}}$ can be easily translated into a quantum circuit. Modern languages such as Qiskit [9] or Tangelo [10] allow its rapid implementation. The twelve small quantum circuit equivalents can be repeated as many times as desired. The advantage of this approach is that the approximation improves with increasing order K and is robust against errors. The trade-off is that the depth of the circuit

increases rapidly, which poses a challenge for near-term intermediate-scale quantum (NISQ) computers. The presented results used an order $K=128$, which is already very large. A scheme of the Doktorov operator trotterized to an order K is shown on Figure 2.

3.3. Hybrid SWAP method

Now that the excited vibrational wavefunction can be changed to a different basis, the overlap between the initial ground state and the final excited state wavefunctions needs to be calculated. To achieve this, the SWAP method was implemented [12]. It is a hybrid method that consists of a Bell measurement followed by a classical post-treatment. This method has the advantage of having a constant complexity. The final ansatz with the SWAP circuit is shown on Figure 3.

The final quantum measurement follows a dot product with the post-treatment vector $\vec{c} = (1, 1, 1, -1)^{\otimes 2LM}$. At the end, the resulting number is the FC factor

$$FC_{1 \rightarrow 2} = \left| \langle \psi_{2i}^{\text{vib}} | \hat{U}_{\text{Dok}} | \psi_{1i}^{\text{vib}} \rangle \right|^2.$$

To obtain the entire absorption spectra, this procedure must be repeated for all vibronic states. No special pre-screening was conducted to determine the vibronic states of interest beforehand. However, it was estimated through

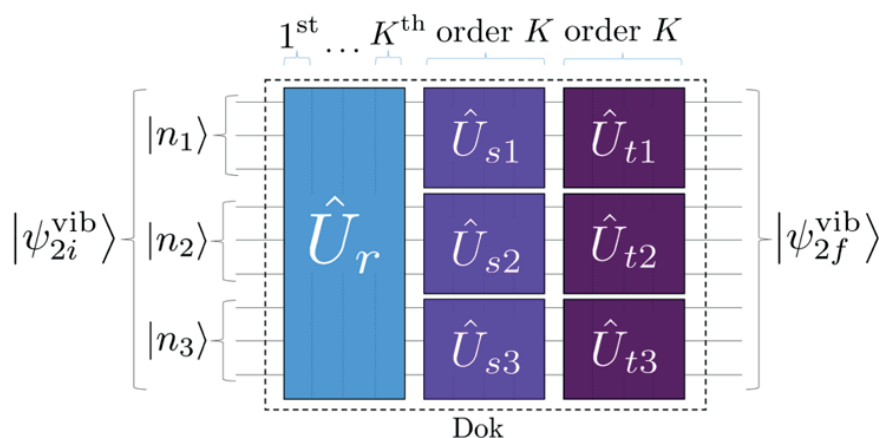


Figure 2 - Scheme of the Doktorov circuit trotterized up to order K . The vibrational wavefunction has three normal modes, each truncated to three qubits. Adapted from ref. [11].

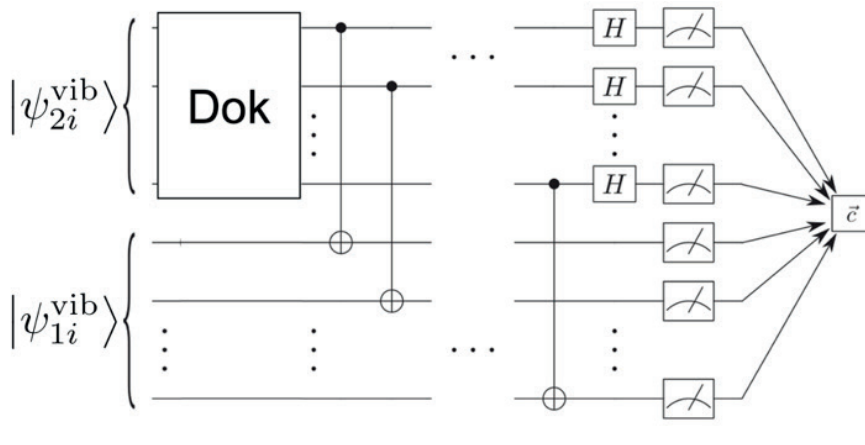


Figure 3 - Doktorov and SWAP circuits combined as final ansatz. Adapted from ref. [11].

previous simpler calculations, notably using a small trotterization, that four qubits were sufficient to adequately represent the spectra of the studied molecules. By monitoring the sum of the Franck-Condon (FC) factors, which should equal one, the quality of the spectra was continuously monitored. The results herein kept 99% of the vibrational intensity for the SO_2 molecule, and 97% for the ZnOH molecule. The simulation was done using the *state-vector* back end.

4. Results and discussions

The results presented herein are ionizations for the SO_2 and ZnOH molecules. These molecules were chosen based on the availability of their Duschinsky matrices and simulated spectra. Another significant factor is that these molecules belong to different symmetry point groups. The parameters used are presented in Table 1.

The first case is the SO_2 molecule, see Fig. 4 (a). Sawaya and Huh [13] simulated the ionization absorption spectrum using the classical Density Functional Theory (DFT) at the B3LYP/6-311+G(3df) level, and the ideal Quantum Fourier Transformation (QFT). Their results followed a Lorentzian broadening (grey line) and are considered as a reference. Indeed, QFT is a very accurate method, but it is also highly resource demanding. For instance, for the same number of normal modes, or qubits, QFT scales quadratically, whereas the presented approach, without rotational mixing, grows linearly. The simulated vibrational intensities (blue peaks) closely reproduce the reference using 15 vibrational states. This first example represents the simplest model with a few vibrational states that validate the method.

Ionization	α	β	θ (rad)
$\text{SO}_2^- \rightarrow \text{SO}_2 + e^-$ [13]	-1.3313	0.0556	-0.0646
	0.3218	0.0275	
	0	0.0476	
$\text{ZnOH}^- \rightarrow \text{ZnOH} + e^-$ [14]	1.3950	0.0921	0.2526
	0.2265	0.0606	
	-0.0229	0.0043	

Table 1. Summary of the Parameters for the Different Ionizations

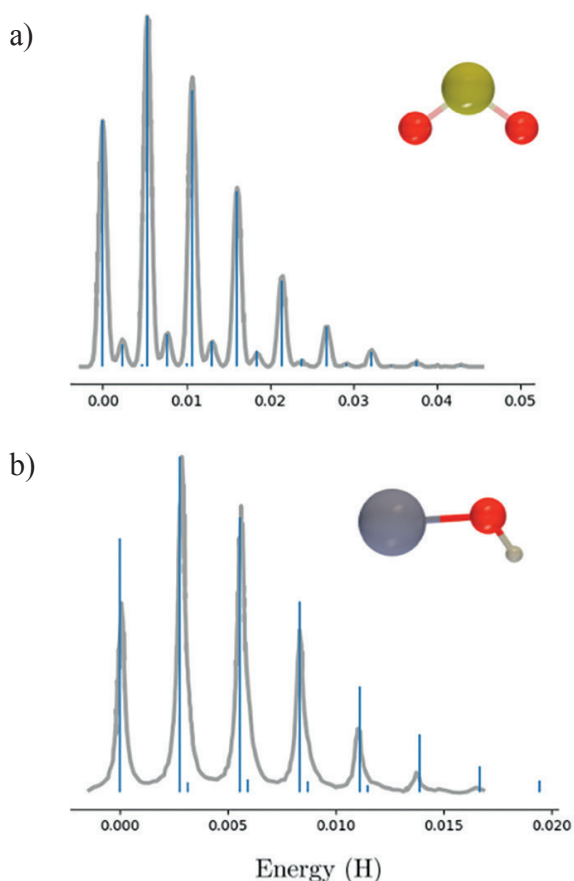


Figure 4 - Comparison between the Dirac-like Franck-Condon factors issued from the present work (blue vertical lines) and the simulated spectra from Sawaya and Huh [13] (a, SO₂) and Meier and Rauhut [14] (b, ZnOH). The intensities have been normalized to arbitrary units and adjusted so that the highest peaks of this work and of the references match. Adapted from ref. [11].

The second example is the ZnOH molecule depicted in Fig. 4 (b). Meier and Rauhut [14] considered relativistic effects using the ECP10MDF effective core potential and the CCSD(T)/6-311++G(3df,2pd) level of theory. Their work uses the multidimensional integral (MDI) method to obtain the absorption spectrum accounting for anharmonic corrections. The resulting curve was entirely produced by classical computer algorithms and is used as a reference (grey line). The 12 simulated intensities (blue peaks) generally follow the trend of the spectrum. However, the deviation becomes slightly more pronounced at higher energies. The estimated Franck-Condon (FC) factors are overestimated, as expected from the pure harmonic approximation used in the methodology. A simpler explanation is that the reference curve incorporates a more complete theoretical framework.

Nevertheless, simulating a three-atomic molecule with a symmetry other than C_{2v} represents an achievement among quantum computer algorithms. The method demonstrates flexibility and generality in simulating vibronic spectra using quantum algorithms. Instead of computing individual normal mode spectra and then mixing them, this algorithm directly mixes and computes the complete vibrational tensor.

4. Conclusions

The work presented here calculates Franck-Condon factors using a hybrid quantum algorithm to simulate UV-vis absorption spectra resulting from ionizations. The studied molecules serve as a proof of concept for the algorithm, demonstrating its symmetry-independence. To our knowledge, this is the first general algorithm applicable to molecules of any size and type. However, despite the robustness of the trotterization method against errors, the quantum circuit size is currently unfeasible for current NISQ machines. Trotterization rapidly increases the circuit depth, and the extensive measurements required for all normal modes are the primary limitations of the method. Nevertheless, it remains a promising approach for vibronic structure calculations and a highly flexible tool that can be integrated with other methods to exploit the vast vibronic Hilbert space more effectively. Future work includes extending the method to electronic transitions, larger molecules, and incorporating anharmonic corrections, which is currently underway.

This work is considered as a more accessible vulgarisation of the original article [11] where the curious reader is referred for more detailed and complete explanations.

References

- [1] F. Arute, K. Arya, R. Babbush, D. Bacon, J. C. Bardin, R. Barends, R. Biswas, S. Boixo, F. G. S. L. Brandao, D. A. Buell, B. Burkett, Y. Chen, Z. Chen, B. Chiaro, R. Collins, W. Courtney, A. Dunsworth, E. Farhi, B. Foxen, A. Fowler, C. Gidney, M. Giustina, R. Graff, K. Guerin, S. Habegger, M. P. Harrigan, M. J. Hartmann, A. Ho, M. Hoffmann, T. Huang, T. S. Humble, S. V. Isakov, E. Jeffrey, Z. Jiang, D. Kafri, K. Kechedzhi, J. Kelly, P. V. Klimov, S. Knysh, A. Korotkov, F. Kostritsa, D. Landhuis, M. Lindmark, E. Lucero, D. Lyakh, S. Mandrà, J. R. McClean, M. McEwen, A. Megrant, X. Mi, K. Michielsen, M. Mohseni, J. Mutus, O. Naaman, M. Neeley, C. Neill, M. Y. Niu, E. Ostby, A. Petukhov, J. C. Platt, C. Quintana, E. G. Rieffel, P. Roushan, N. C. Rubin, D. Sank, K. J. Satzinger, V. Smelyanskiy, K. J. Sung, M. D. Trevithick, A. Vainsencher, B. Villalonga, T. White, Z. J. Yao, P. Yeh, A. Zalcman, H. Neven and J. M. Martinis, “Quantum supremacy using a programmable superconducting processor,” *Nature*, vol. 574, p. 505–510, October 2019.
- [2] S. McArdle, S. Endo, A. Aspuru-Guzik, S. C. Benjamin and X. Yuan, “Quantum computational chemistry,” *Rev. Mod. Phys.*, vol. 92, p. 015003, March 2020.
- [3] P. J. Ollitrault, A. Kandala, C.-F. Chen, P. K. Barkoutsos, A. Mezzacapo, M. Pistoia, S. Sheldon, S. Woerner, J. M. Gambetta and I. Tavernelli, “Quantum equation of motion for computing molecular excitation energies on a noisy quantum processor,” *Phys. Rev. Res.*, vol. 2, p. 043140, October 2020.
- [4] M. Bruschi, F. Gallina and B. Fresch, “A Quantum Algorithm from Response Theory: Digital Quantum Simulation of Two-Dimensional Electronic Spectroscopy,” *J. Phys. Chem. Lett.*, vol. 15, p. 1484–1492, January 2024.
- [5] N. P. D. Sawaya, F. Paesani and D. P. Tabor, “Near- and long-term quantum algorithmic approaches for vibrational spectroscopy,” *Phys. Rev. A*, vol. 104, p. 062419, December 2021.
- [6] C. S. Wang, J. C. Curtis, B. J. Lester, Y. Zhang, Y. Y. Gao, J. Freeze, V. S. Batista, P. H. Vaccaro, I. L. Chuang, L. Frunzio and others, “Quantum simulation of molecular vibronic spectra on a superconducting bosonic processor,” *arXiv:1908.03598*, 2019.
- [7] S. McArdle, A. Mayorov, X. Shan, S. Benjamin and X. Yuan, “Digital quantum simulation of molecular vibrations,” *Chem. Sci.*, vol. 10, p. 5725–5735, 2019.
- [8] J. E. Cohen, S. Friedland, T. Kato and F. P. Kelly, “Eigenvalue inequalities for products of matrix exponentials,” *Linear Algebra Appl.*, vol. 45, p. 55–95, June 1982.
- [9] G. Aleksandrowicz, T. Alexander, P. Barkoutsos, L. Bello, Y. Ben-Heim, D. Bucher, F. J. Cabrera-Hernández, J. Y. Carballo-Franquis, A. Chen, C.-F. Chen and e. al., *Qiskit: An Open-source Framework for Quantum Computing*, 2021.
- [10] V. Senicourt, J. Brown, A. Fleury, R. Day, E. Lloyd, M. P. Coons, K. Bieniasz, L. Huntington, A. J. Garza, S. Matsuura, R. Plesch, T. Yamazaki and A. Zaribafiyani, *Tangelo: An Open-source Python Package for End-to-end Chemistry Workflows on Quantum Computers*, 2022.
- [11] R. Olarte Hernandez, B. Champagne and A. Soldera, “Simulating Vibronic Spectra by Direct Application of Doktorov Formulas on a Superconducting Quantum Simulator,” *J. Phys. Chem. A*, vol. 128, p. 4369–4377, May 2024.
- [12] L. Cincio, Y. Subaşı, A. T. Sornborger and P. J. Coles, “Learning the quantum algorithm for state overlap,” *New J. Phys.*, vol. 20, p. 113022, November 2018.
- [13] N. P. D. Sawaya and J. Huh, “Quantum Algorithm for Calculating Molecular Vibronic Spectra,” *J. Phys. Chem. Lett.*, vol. 10, p. 3586–3591, June 2019.
- [14] P. Meier and G. Rauhut, “Comparison of methods for calculating Franck–Condon factors beyond the harmonic approximation: how important are Duschinsky rotations?,” *Mol. Phys.*, vol. 113, p. 3859–3873, September 2015.
- [15] M. A. Nielsen and I. L. Chuang, *Quantum Computation and Quantum Information*, Cambridge: Cambridge University Press, 2000.



Thomas CARABIN* and Anne-Sophie DUWEZ

UR Molecular Systems, University of Liège,
Sart-Tilman 4000, Belgium
NANO-CHEM, Department of Chemistry, University of Liège,
Quartier Agora, Allée du Six Août 14, B18, Sart-Tilman,
4000 Liège.
Phone number: 0484386356
t.carabin@uliege.be

Investigating the mechanical stability of Diels-Alder mechanophores by AFM-based single-molecule force spectroscopy

Abstract

Mechanical activation of chemical bonds is a fundamental process in nature but remains underutilized in chemistry and material science [1,2]. Utilizing mechanical forces to induce chemical reactions in materials, particularly by incorporating mechanophore molecules, which contain scissile bonds that undergo predictable and detectable rupture under stress, offers opportunities to design stress-responsive materials [3]. These developments are made possible by a deep understanding of the mechanochemical behaviour of the mechanophores. Here, we describe how atomic force microscopy-based single-molecule force spectroscopy (AFM-SMFS), a technique which enables the precise and quantitative mechanical study of individual molecules, can provide invaluable information on the influence of their regio- and stereochemistry on their mechanical behaviour. We report on an ongoing project on the furan-maleimide Diels-Alder (fmDA)

mechanophore. This adduct presents dynamic covalent bonds and can have four different geometries that differ by their regio- (proximal or distal) and stereochemistry (endo or exo), which makes it a good candidate for creating intelligent materials driven by mechanical forces.

Keywords

Mechanochemistry, mechanophore, single-molecule force spectroscopy, Diels-Alder.

1. Polymer mechanochemistry and mechanophores

Mechanochemistry can be related to chemical reactions triggered by the application of mechanical stress. Traditionally, mechanical constraints have been regarded as destructive, causing chemical rupture in materials, and limiting their applications. However, in the early 2000s [3], a new perspective emerged,

suggesting that mechanical forces could be used in a productive way, enabling the creation of mechanoresponsive polymer materials. This conceptual shift in mechanochemistry has been particularly explored through the design, study, and application of “mechanophore” entities.

Mechanophores are entities that react predictably to mechanical forces by emitting a detectable signal. This response typically involves a conformational change or the breaking of scissile bonds under an applied force. Key examples include Diels-Alder [4,5] (Figure 1a) and spiropyran [6,7] mechanophores (Figure 1b), where the scissile covalent bonds are C–C and C–O, respectively.

Over the past decades, many mechanophores presenting different mechanochemical properties have been developed to create new stress-responsive materials. The first example concerned mechanophores that can change their optical properties under mechanical constraints. This optical response manifests itself as a change in visible color [8,9], fluorescence [10,11], or phosphorescence [12,13]. This property enables the creation of optical force-detecting devices for sensing deformation or local stress in materials and quick reaction to avoid a potential failure. Some mechanophores can also act as latent catalysts when embedded in materials [14,15]. These adducts present an inactive and stable “locked” state until activated by an external force. It results in the release of catalytic species that can be used to trigger specific reactions

on demand. With this idea, a large panel of small molecules can also be released thanks to a specific design of mechanophores. This small molecule release can proceed directly during the mechanochemical reaction [16,17] of the mechanophore or by the spontaneous decomposition of the product resulting from this transformation [18,19]. These examples show the possibility of mechanophores playing a significant role in the creation of a new generation of intelligent materials and logic devices driven by mechanical forces. However, to allow these applications we need to identify the key parameters governing the mechanical response of these mechanophore structures, such as their rupture force or rupture mechanism and the influence of their molecular structure and environment. AFM-based single-molecule force spectroscopy (SMFS) has proven to be an efficient method to obtain this precise and quantitative information by allowing the evaluation of the mechanochemical behaviour of individual molecules. Here, we will briefly describe the basic principle of SMFS and show how it can contribute to obtain a detailed picture of the mechanical behaviour of Diels-Alder mechanophores.

2. AFM-based single molecule force spectroscopy

An example of an AFM setup is illustrated in Figure 2. A cantilever with a tip at its end is positioned above a surface sample and placed on a piezoelectric scanner, enabling precise three-dimensional movement. As the sample approaches

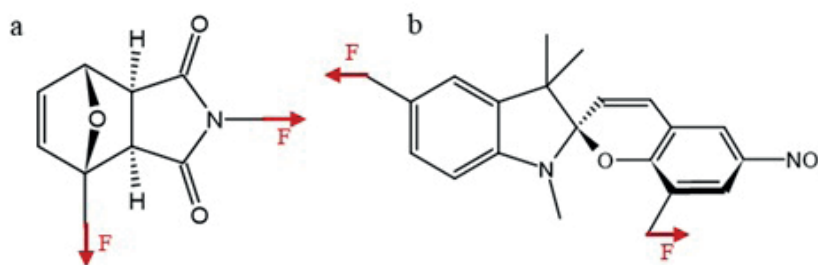


Figure 1: Chemical structure of furan-maleimide Diels-Alder (a), and spiropyran (b) mechanophores. The potential application of force is shown in red.

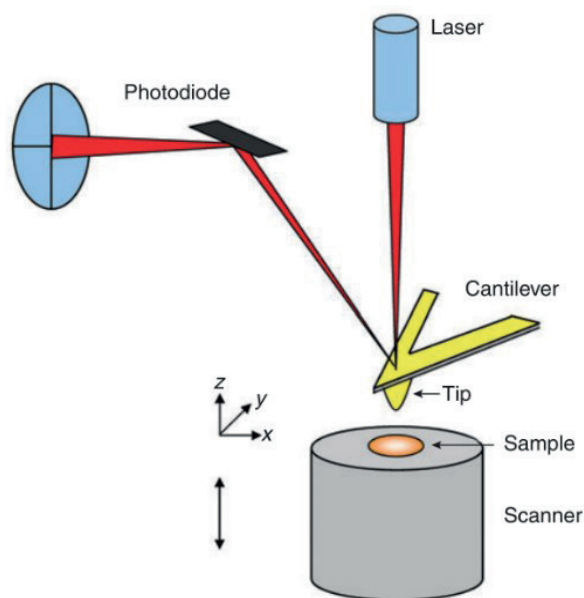


Figure 2: Schematic representation of an atomic force microscope [20].

the tip, interaction forces occur between the tip and the surface, causing the cantilever to bend. This bending is monitored using a laser beam aimed at the end of the cantilever, where it is reflected and is subsequently detected by a photodiode. The cantilever's spring constant is a key property, enabling the conversion of the detected deflection into the force exerted on the tip, as determined by Hooke's law.

During AFM-based single-molecule force spectroscopy (SMFS), a single molecule is trapped and stretched between the tip and the surface. The detailed process of molecule stretching during SMFS is illustrated in Figure 3. First, the surface, grafted with a very low amount of molecule of interest, is brought into contact with the tip. During the contact, interactions between a single molecule and the tip can take place. The surface is then retracted, and if a molecule attached to the tip during contact, it will be trapped and the force increases parabolically as the molecule resists stretching. This continues until the weakest link in the system (tip + molecule + surface) breaks, creating a force peak profile. After this rupture event, the cantilever returns to its zero-force equilibrium position, and the

surface is repositioned for the next approach/retraction cycle. The data collected consists of the cantilever deflection (measured in volts, reflecting the laser beam movement on the photodiode) relative to the piezo scanner's position (in nanometers). This raw data can be converted into the force exerted on the cantilever as a function of the separation distance between the tip and the surface. Each cantilever is characterized by a deflection sensitivity, which relates nanometer-scale cantilever deflection (d) to the laser displacement on the photodiode through the following equation (Equ. 1):

$$d = V \cdot S \quad (1)$$

where V is the detected displacement of the laser beam (in volts) and S is the deflection sensitivity of the cantilever (in nm.volt^{-1}). The separation between the tip and the surface (z) can be calculated by withdrawing this distance (d) to the displacement of the piezo scanner (z_0), thanks to Equ.2.

$$z = z_0 - d \quad (2)$$

Finally, the force exerted on the cantilever (F) is determined using Hooke's law by multiplying the cantilever's deflection (d) by its spring constant (k):

$$F = d \cdot K \quad (3)$$

The analysis of force-distance curves and the occurrence of rupture events provide insights into intermolecular and intramolecular interactions, conformational transitions, mechanochemical behaviour, and more. Therefore, it makes SMFS an effective method to study mechanophores [21-28], mechanically interlocked molecules [29,30], and other non-trivial small molecules [31,32], among others.

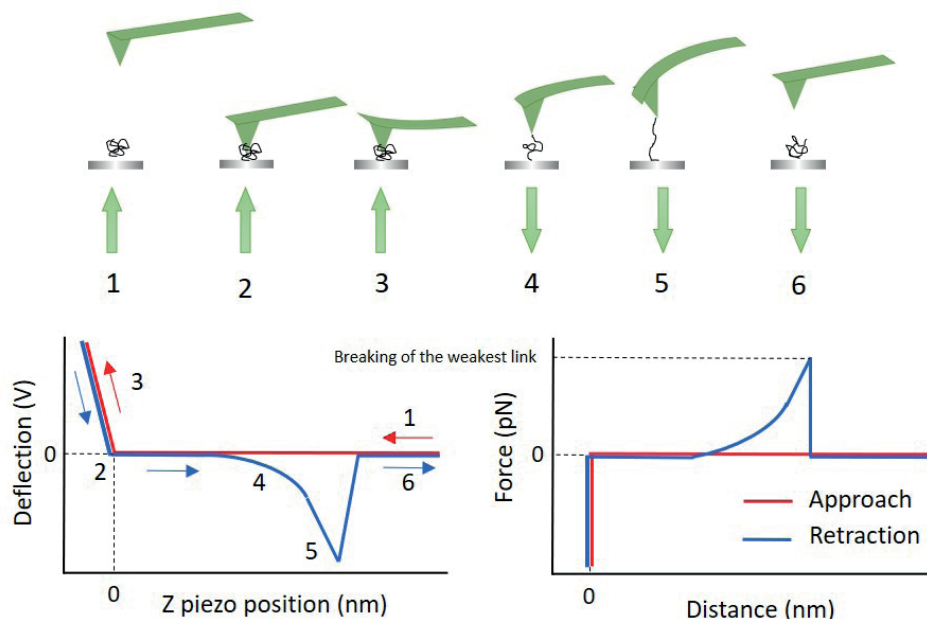


Figure 3: Schematic illustration of a single-molecule force spectroscopy experiment on a molecule and transformation of the obtained deflection-piezo position curve into a force-distance curve.

3. Investigation of the mechanical behaviour of the furan-maleimide Diels-Alder mechanophore

In the NanoChem research group, we are currently investigating the mechanical properties of the mechanophore formed through the archetypal Diels-Alder reaction between a furan and a maleimide moiety (fmDA mechanophore). This project is motivated by several factors. The Diels-Alder reaction is both straightforward and atom-efficient, and since furan derivatives can be sourced from biomass, this [4+2] cycloaddition is increasingly recognized as a key process in green chemistry [33]. Additionally, the fmDA mechanophore can undergo a retro-Diels-Alder reaction at moderately high temperature [34], making it highly relevant for polymer science, particularly for tailoring polymer properties.

The furan/maleimide Diels-Alder (fmDA) adduct has been incorporated into a wide range of polymer and composite materials [35-38], including hydrogels, coatings, and multifunctional materials with applications in self-healing, shape memory, thermal reprocessing, chemical recycling, and drug delivery. Furthermore, the fmDA mechanophore's mechanical properties

make it an excellent candidate for polymer mechanochemistry. For example, stimuli-responsive polymers capable of releasing small molecules under mechanical stress have been created using this mechanophore [19].

Despite numerous interesting applications, quantitative/experimental precise data on the mechanochemical behaviour of the fmDA mechanophore remain limited. A few mechanical studies using ultra-sounds have been already made on this mechanophore suggesting that its geometry (stereo and regiochemistry) affects its mechanochemical behaviour [39-41]. However, quantitative information such as the rupture force or the rupture mechanism of this mechanophore, which are key parameters for its applications, is still lacking. To address this lack, we use AFM-based single-molecule force spectroscopy to study four geometries of the fmDA mechanophore (proximal-endo, proximal-exo, distal-endo, and distal-exo) (Figure 4). The adducts are synthesized by the group of Guillaume De Bo, University of Manchester, UK, who synthesized and incorporated the mechanophores into polymer systems used as linkers during SMFS experiments (Figure 5). The primary goals of

these experiments are to measure the rupture force of the fmDA adducts and elucidate their rupture mechanisms at the single-molecule level, using advanced modes of SMFS, such as force clamp experiments. By comparing the mechanical responses of the different geometries, we aim to identify the relationship between molecular properties and the mechanical stability of the fmDA mechanophores.

4. Conclusions and perspectives

The results show that the presence of a long polymer linker leads to a delayed propagation of

the external force to the mechanophore during stretching, increasing its exposition time and rupture probability at low forces. The amplitude of the rupture force depends on the geometry of the adduct. The distal-exo one was shown to be mechanoresistant. Distance-clamp experiments enabled to obtain information on the rupture mechanism, evidencing a concerted or sequential mechanism, depending on the geometry. This work confirms the impact of external forces on the chemical behaviour of mechanophores, which can result in an acceleration of their rupture or a modification of their thermal rupture mechanism.

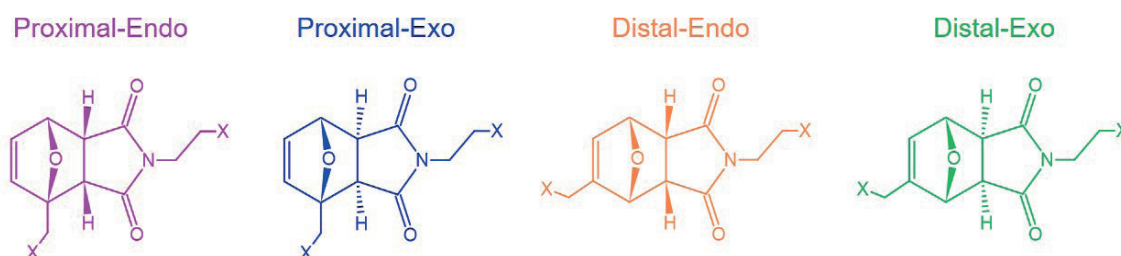


Figure 4: Furan-maleimide mechanophore geometries depending on its stereochemistry and regiochemistry.

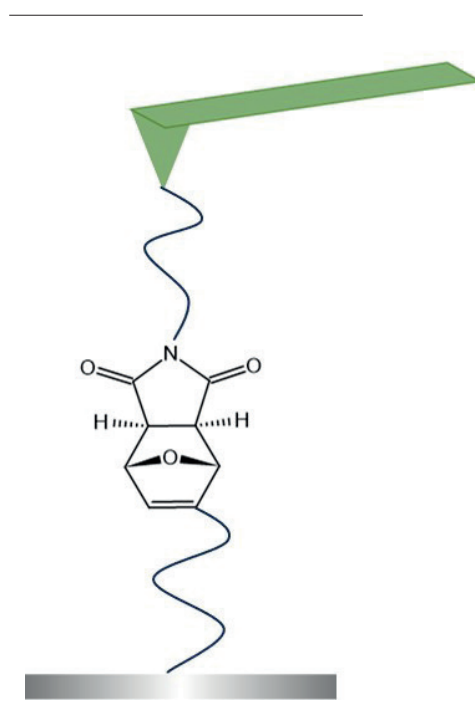


Figure 5: Schematic view of AFM-based single molecule force spectroscopy (SMFS) pulling experiment on the fmDA mechanophore incorporated in a polymer chain.

References

- [1] Camp, R. J.; Liles, M.; Beale, J.; Saeidi, N.; Flynn, B. P.; Moore, E.; Murthy, S. K.; Ruberti, J. W. *Journal of the American Chemical Society*, 2011, 133, 4073–4078.
- [2] Bloom, K. S. *Chromosoma*, 2007, 117, 103–110.
- [3] Li, J.; Nagamani, C.; Moore, J. S. *Accounts of Chemical Research*, 2015, 48, 2181–2190.
- [4] Stevenson, R.; De Bo, G. *Journal of the American Chemical Society*, 2017, 139, 16768–16771.
- [5] Duan, H.-Y.; Wang, Y.-X.; Wang, L.-J.; Min, Y.-Q.; Zhang, X.-H.; Du, B.-Y. *Macromolecules*, 2017, 50, 1353–1361.
- [6] Gossweiler, G. R.; Kouznetsova, T. B.; Craig, S. L. *Journal of the American Chemical Society*, 2015, 137, 6148–6151.
- [7] Li, M.; Zhang, Q.; Zhou, Y.-N.; Zhu, S. *Progress in Polymer Science*, 2018, 79, 26–39.
- [8] Davis, D. A.; Hamilton, A.; Yang, J.; Cremer, L. D.; Van Gough, D.; Potisek, S. L.; Ong, M. T.; Braun, P. V.; Martínez, T. J.; White, S. R.; Moore, J. S.; Sottos, N. R. *Nature*, 2009, 459, 68–72.
- [9] Beiermann, B. A.; Kramer, S. L. B.; Moore, J. S.; White, S. R.; Sottos, N. R. *Role of ACS Macro Letters*, 2011, 1, 163–166.
- [10] Traeger, H.; Sagara, Y.; Kiebal, D. J.; Schrettl, S.; Weder, C. *Angewandte Chemie International Edition*, 2021, 60, 16191–16199.
- [11] Chen, Y.; Yeh, C. J.; Qi, Y.; Long, R.; Creton, C. *Science Advances*, 2020, 6.
- [12] Filonenko, G. A.; Khusnutdinova, J. R. *Advanced Materials*, 2017, 29.
- [13] Filonenko, G. A.; Lugger, J. A. M.; Liu, C.; van Heeswijk, E. P. A.; Hendrix, M. M. R. M.; Weber, M.; Müller, C.; Hensen, E. J. M.; Sijbesma, R. P.; Pidko, E. A. *Angewandte Chemie International Edition*, 2018, 57, 16385–16390.
- [14] Michael, P.; Sheidaee Mehr, S. K.; Binder, W. H. *Journal of Polymer Science Part A: Polymer Chemistry*, 2017, 55, 3893–3907.
- [15] Wei, K.; Gao, Z.; Liu, H.; Wu, X.; Wang, F.; Xu, H. *ACS Macro Letters*, 2017, 6, 1146–1150.
- [16] Larsen, M. B.; Boydston, A. J. *Journal of the American Chemical Society*, 2013, 135, 8189–8192.
- [17] Shen, H.; Larsen, M. B.; Roessler, A. G.; Zimmerman, P. M.; Boydston, A. J. *Angewandte Chemie International Edition*, 2021, 60, 13559–13563.
- [18] Diesendruck, C. E.; Steinberg, B. D.; Sugai, N.; Silberstein, M. N.; Sottos, N. R.; White, S. R.; Braun, P. V.; Moore, J. S. *Journal of the American Chemical Society*, 2012, 134, 12446–12449.
- [19] Hu, X.; Zeng, T.; Husic, C. C.; Robb, M. J. *Journal of the American Chemical Society*, 2019, 141, 15018–15023.
- [20] Hinterdorfer, P.; Dufrière, Y. F. *Nature Methods*, 2006, 3, 347–355.
- [21] Wu, D.; Lenhardt, J. M.; Black, A. L.; Akhremitchev, B. B.; Craig, S. L. *Journal of the American Chemical Society*, 2010, 132, 15936–15938.
- [22] Wang, J.; Kouznetsova, T. B.; Niu, Z.; Ong, M. T.; Klukovich, H. M.; Rheingold, A. L.; Martínez, T. J.; Craig, S. L. *Nature Chemistry*, 2015, 7, 323–327.
- [23] Klukovich, H. M.; Kouznetsova, T. B.; Kean, Z. S.; Lenhardt, J. M.; Craig, S. L. *Nature Chemistry*, 2012, 5, 110–114.
- [24] Wang, J.; Kouznetsova, T. B.; Kean, Z. S.; Fan, L.; Mar, B. D.; Martínez, T. J.; Craig, S. L. *Journal of the American Chemical Society*, 2014, 136, 15162–15165.
- [25] Gossweiler, G. R.; Kouznetsova, T. B.; Craig, S. L. *Journal of the American Chemical Society*, 2015, 137, 6148–6151.
- [26] Barbee, M. H.; Kouznetsova, T.; Barrett, S. L.; Gossweiler, G. R.; Lin, Y.; Rastogi, S. K.; Brittain, W. J.; Craig, S. L. *Journal of the American Chemical Society*, 2018, 140, 12746–12750.
- [27] Lin, Y.; Kouznetsova, T. B.; Foret, A. G.; Craig, S. L. *Journal of the American Chemical Society*, 2024, 146, 3920–3925.
- [28] Wang, J.; Kouznetsova, T. B.; Craig, S. L. *Journal of the American Chemical Society*, 2016, 138, 10410–10412.
- [29] (a) Lussis, P.; Svaldo-Lanero, T.; Bertocco, A.; Fustin, C.-A.; Leigh, D. A.; Duwez, A.-S. *Nature Nanotechnology*, 2011, 6, 553–557. (b) Sluysmans, D.; Lussis, P.; Fustin, C.-A.; Bertocco, A.; Leigh, D. A.; Duwez, A.-S. *Journal of the American Chemical Society*, 2021, 143, 2348–2352.
- [30] Sluysmans, D.; Hubert, S.; Bruns, C. J.; Zhu, Z.; Stoddart, J. F.; Duwez, A.-S. *Nature Nanotechnology*, 2018, 13, 209–213.
- [31] Calvaresi, M.; Duwez, A.-S.; Leigh, D. A.; Sluysmans, D.; Song, Y.; Zerbetto, F.; Zhang, L. *Chem*, 2023, 9, 65–75. 79.
- [32] Devaux, F.; Li, X.; Sluysmans, D.; Maurizot, V.; Bakalis, E.; Zerbetto, F.; Huc, I.; Duwez, A.-S. *Chem*, 2021, 7, 1333–1346.
- [33] Galkin, K. I.; Sandulenko, I. V.; Polezhaev, A. V. *Processes*, 2021, 10, 30.
- [34] Gandini, A. *Progress in Polymer Science*, 2013, 38, 1–29.
- [35] Zheng, N.; Xu, Y.; Zhao, Q.; Xie, T. *Chemical Reviews*, 2021, 121, 1716–1745.
- [36] Zhang, Z. P.; Rong, M. Z.; Zhang, M. Q. *Progress in Polymer Science*, 2018, 80, 39–93.
- [37] Briou, B.; Améduri, B.; Boutevin, B. *Chemical Society Reviews*, 2021, 50, 11055–11097.
- [38] Chakma, P.; Konkolewicz, D. *Angewandte Chemie International Edition*, 2019, 58, 9682–9695.
- [39] Stevenson, R.; De Bo, G. *Journal of the American Chemical Society*, 2017, 139, 16768–16771.
- [40] Wang, Z.; Craig, S. L. *Chemical Communications*, 2019, 55, 12263–12266.
- [41] Cardosa-Gutierrez, M.; De Bo, G.; Duwez, A.-S.; Remacle, F. *Chemical Science*, 2023, 14, 1263–1271.

Pour vous faire membre de la SRC et accéder gratuitement à la revue Chimie Nouvelle :

il vous suffit de verser au compte BNP Paribas Fortis : BE60 2100 4208 0470
la somme indiquée dans le tableau ci-dessous :

Membres résidant en Belgique et au Luxembourg

Membres effectifs : **60 euros**

- participation gratuite ou à prix réduit à toutes les activités de la SRC
- abonnement gratuit à la revue "Chimie Nouvelle"
- accès gratuit à la bibliothèque de la SRC.

Membres associés : **30 euros**

- Réservé, avec les mêmes avantages que les membres effectifs, aux personnes âgées de moins de 30 ans, aux professeurs de l'enseignement secondaire et aux retraités.

Membres Juniors : Gratuit

- Réservé aux étudiants du 2^e cycle universitaire et des écoles d'ingénieurs industriels et aux étudiants de dernière année des graduats en chimie et biochimie avec les mêmes avantages que les membres effectifs

Membres résidant à l'étranger

Membres effectifs : **60 euros**

Membres associés : **30 euros**